ELSEVIER

Catalysis Today 23 (1995) 283–298

CATALYSIS TODAY

A sub-nanometer structural study of Pt–Rh catalysts supported on Ce doped SiC

M. Benaïssa [a,b,1], C. Pham-Huu [a], J. Werckmann [b], C. Crouzet [a], M.J. Ledoux [a,*]

[a] *Laboratoire de Chimie des Matériaux Catalytiques, EHICS, 1 rue Blaise Pascal, 67008 Strasbourg Cédex, France*

[b] *IPCMS-GSI, UMR 46 CNRS, 23 rue du Loess, 67037 Strasbourg Cédex, France*

Abstract

In this paper, the HRTEM technique has been applied to the structural study of Pt–Rh catalysts supported on Ce doped SiC. The results on cerium doped active carbon and on cerium doped silicon carbide synthezised before its use as catalyst support are also reported. It was found that the Ce doped SiC catalyst support contains a new compound which is a Ce amorphous phase. The presence of such a compound within the support is thought to have the advantage of contributing to the improvement of the activity of the catalysts. At present, the HRTEM study on reduced Pt–Rh/SiC–Ce catalyst gives direct evidence of a selective association of Pt and Rh metals with the cerium oxide additive. This association, on the one hand, shows that cerium oxide is not inert towards noble metals, and on the other hand, it gives rise to a noble metal–cerium oxide composite to which the reduction is linked. The formation of an active interface, or a buffer oxygen layer which can be defined as a surface that serves as a common boundary between noble metals and cerium oxide, must be then considered in order to interpret the improvement in catalytic activities. After the ageing treatment, some structural changes were observed, particuiarly the formation a Rh sub-oxide phase formed by three to four monoatomic layers. Finally, it seems that the main oxidation and reduction processes occur through the active interface where the cerium oxide is easily able to change from cerium plus four (Ce^{4+}) to cerium plus three (Ce^{3+}) oxidation state. The metal will act only as a donor or acceptor of electrons. It must be emphasised that the SiC catalyst support showed a high chemical inertia since no structural modifications were observed on the noble metals caused by SiC.

1. Introduction

Due to its chemical inertness and high thermal resistance, silicon carbide (SiC) is a highly promising candidate as a support material for many potential commercial catalytic applications (exhaust emission control etc.). Using a new synthetic route developed by Ledoux et al. [1,2], it is possible to obtain cerium doped silicon carbides with high specific-surface-area for use as supports for active phases (Pt + Rh).

Ceria (CeO_2) has been traditionally applied as an additive in three-way conversion (TWC) for commercial catalysts used for the simultaneous conversion of carbon monoxide (CO), hydrocarbons (HC) and nitrogen oxides (NO_x) in automobile exhausts. The aspect of cerium that has received the most attention is its role as an oxygen storage component in influencing the dynamic behaviour of TWC catalysts under cycled air/fuel ratio conditions [3–7]. In spite of the well established effectiveness of ceria, its role in activity enhancement is still the subject of competing hypotheses. It has gradually became recognised that cerium oxides and the noble metals are subject

* Corresponding author.

[1] Present address: IFUNAM, Depto de Materia Condensada, A.P. 20-346, México D.F. 01000, Mexico.

SSDI 0920-5861(94)00168-5

to mutual interactions, which depend on the nature of the noble metal, the ageing temperature and the gaseous environment. A typical example of this interaction is given in the literature [4], which described the strong enhancement in catalytic activity of reduced Pt–CeO_2 catalysts as a synergism enhancing oxygen storage by the catalyst surface.

In fact, the exact nature of the interaction is not well understood, although several hypotheses such as formation of Pt–Ce alloys [8] or promotion of redox reactions over ceria and involvement of anionic vacancies in ceria either for stabilising Pt dispersion [9] or as partial catalytic sites [10], have been proposed. However, these interpretations on a nanometer scale arise from analyses obtained by using macroscopic analytical techniques such as X-ray diffraction, infrared or XPS spectroscopy techniques. The non-homogeneity of the catalyst structure can be a confusing problem. On heterogeneous catalysts, small metal particles are dispersed over support surfaces and the preferred shapes and relationships between these particles and the exposed facets can have a profound impact on the catalytic properties. The use of a technique having a high lateral resolution is needed to provide a model capable of clarifying the complex mechanisms that occur during the conversion reactions.

The last few years have seen the development of high-resolution transmission electron microscopy (HRTEM) techniques for recording surface profile images. The application of this technique to materials science shows great potential because it allows direct information to be obtained on the atomic scale which cannot be gained by normal methods of surface analyses. The activity and selectivity of small metal particle catalysts can be dependent on their crystal size and their surface characteristics. In the field of heterogeneous catalysis, HRTEM provides the possibility of determining changes in the surface on the atomic level before and after catalytic reactions. It is still, however, difficult to observe catalytic reactions within the electron microscope although this is a long-term goal for the future development of microscopy.

The application of HRTEM to Pt–Rh catalysts supported on Ce doped SiC is described in this article. In fact the use of HRTEM gives a clear understanding of the location of the additive and thus a realistic model of the metal–additive interaction. Before focusing on the catalyst, the results on cerium doped active carbon and also on cerium doped silicon carbide synthesised before its use as catalyst–support will also be reported.

2. Experimental

2.1. Synthesis of the catalysts

Silicon carbide powder was prepared by reacting a silicon monoxide (SiO) vapour with a high-specific-surface-area active carbon, as follows:

$$SiO_{gas} + 2C_{solid} \Leftrightarrow SiC_{solid} + CO_{gas} \quad (1)$$

The reaction was carried out under reduced pressure of SiO ($P_{SiO} = 0.6$ mbar) at 1240°C for 7 h. Full details of the synthesis of the undoped carbide are reported elsewhere [1,2]. The microstructure of the active carbon and the growth of SiC have previously been studied by HRTEM [11,12].

The present study focuses the investigation on the doped catalyst. In fact, before SiC synthesis, the active carbon can be doped with different additives. Here, the doping agent is cerium (Ce). Cerium is introduced into the active carbon by the incipient wetness method using an aqueous solution of ammonium ceric nitrate $Ce(NO_3)_3(NH_4)_2$ (*Aldrich*). In order to estimate the dispersion of the Ce particles within the active carbon, HRTEM observations were performed on a heat-treated Ce doped active carbon sample (at 1240°C for 7 h) and are reported below. The Ce doped SiC catalyst–support was obtained by reacting the Ce doped active carbon with SiO.

The metals were deposited by dissolving metal salts [$Pt(NH_3)_4Cl_2,H_2O$] and [$Rh(NO_3),2H_2O$] (*Strem-Chemicals*) in a solvent followed by

incipient wetness of the dried support. The platinum (Pt) solution was deposited first. After drying at 120°C for 14 h, the catalyst was calcinated in air at 500°C for 2 h. Then, rhodium (Rh) solution was added and similar treatments, as for platinum, were undertaken. Before catalytic cycling, the obtained catalyst (1 wt.-% Pt–0.2 wt.-%Rh)/(SiC–5 wt.-% Ce) was reduced in situ in H_2 flowing (40 cm^3 min^{-1}) at 450°C for 2 h.

Catalysts (with and without Ce) were evaluated by studying their light-off behaviour in simulated exhaust gas mixtures (CO, NO and HC) from 50°C to 500°C at a heating rate of 5°C/min and a VVH of 37500 h^{-1}. The conversion efficiencies of the catalyst were measured by continuously monitoring the outlet gases after the catalyst. The composition of the simulated exhaust gas to achieve a mixture is as follows: CO = 5700 ppm, NO = 2050 ppm, HC = 950 ppm (C_3H_8 = 238 ppm and C_3H_6 = 712 ppm), O_2 = 6200 ppm and nitrogen at atmospheric pressure.

Catalytic tests were conducted on: (a) a reduced catalyst, on (b) sample (a) after calcination in air at 800°C for 16 h under 4% water vapour and finally on (c), sample (b) after calcination in air at 1000°C for 10 h under 4% water vapour. Only samples (a) and (c) were characterised by HRTEM. Extreme b and c treatments were performed to simulate ageing of a catalyst used under normal conditions for more than 50000 miles.

The beneficial change when using cerium oxide as an additive was demonstrated in the form of light-off curves for NO and CO conversion [13]. A clear improvement of CO and NO conversion was observed both in yield and light-off temperature drop.

2.2. *HRTEM characterisation*

HRTEM combined with energy dispersive X-ray microanalysis (EDX) were carried out by using a Topcon EM002B electron microscope (200 keV) equipped with a Kevex analytical system. Samples were supported on holey carbon-coated copper grids by simply grinding the specimen between glass plates and bringing the powder into contact with the grid. To prevent artefacts due to contamination, no solvents were used at any stage of the sample preparation. Great care was taken during HRTEM experiments in order to avoid heating effects from the electron beam. The samples were quite stable so that micrographs could be recorded at magnifications of 590 000×. The magnification of the HRTEM images and the optical diffractograms were all calibrated under the same electron-optical conditions. Complementary EDX microanalysis was used to check the chemical composition of the particle under

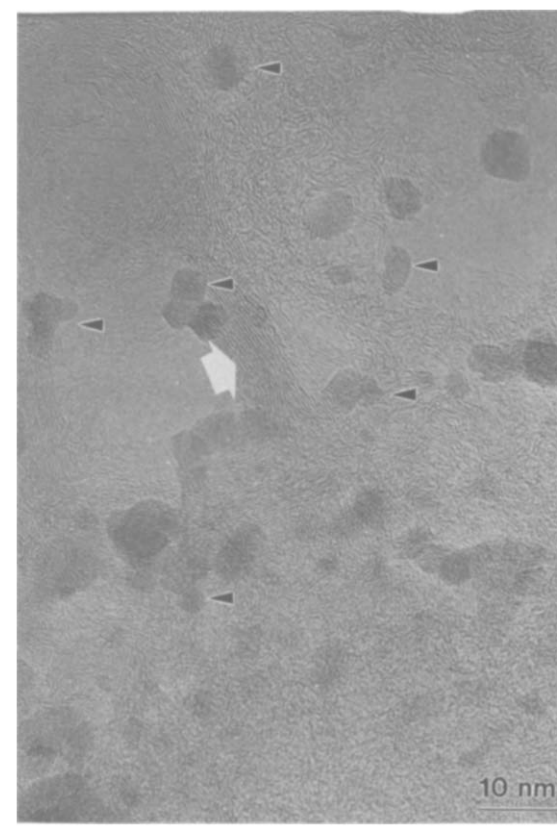

Fig. 1. A typical low-magnification image of the heat-treated cerium doped active carbon. The image shows a good dispersion of cerium oxide particles over the active carbon. The cerium oxide particles (arrows) are present in CeO_2 cuboctahedral shape, while the active carbon is slightly organised (white arrow).

observation. The spectra are not reported (see ref. [13]).

3. Results and discussion

3.1. Heat-treated cerium doped active carbon

A typical low-magnification electron micrograph of the cerium doped active carbon after it had been heat-treated at 1240°C for 7 h is shown in Fig. 1. The cerium oxide particles (arrows) are often present in cuboctahedral forms. The size of these cuboctahedral particles is of the order of 3 to 7 nm. HRTEM observations on some well oriented cerium dioxide (CeO_2) particles are shown in Fig. 2. In Fig. 2a is illustrated a HRTEM micrograph of a typical CeO_2 cuboctahedral particle imaged along the ⟨110⟩ zone axis. The (111), (001) and (110) type facets are easily identified. In Fig. 2b, a similar cuboctahedral particle is observed without presenting the (110) type facets therefore forming perfect (111) dihedra (arrows). It should be noted that no movement of the surface atomic columns was observed during recording the micrographs. The exposure time was equal or less than 1s. It is believed that higher exposure time will effectively induce a complete removal of the unstable (110) type facets; as reported by Cochrane et al. [14] where CeO_2 particles were exposed to the electron beam for more than 30 s. In fact, this dynamical movement can be explained as follows. For a single crystal, the equilibrium configuration is generally governed by the surface energies when these energies are minimised. In the faceted centred cubic structure, the lowest surface energies correspond respectively to (111), (001) and (110) facets [15]. The (110) type facets, in the case of CeO_2, are more susceptible to rearrangement. The rounding

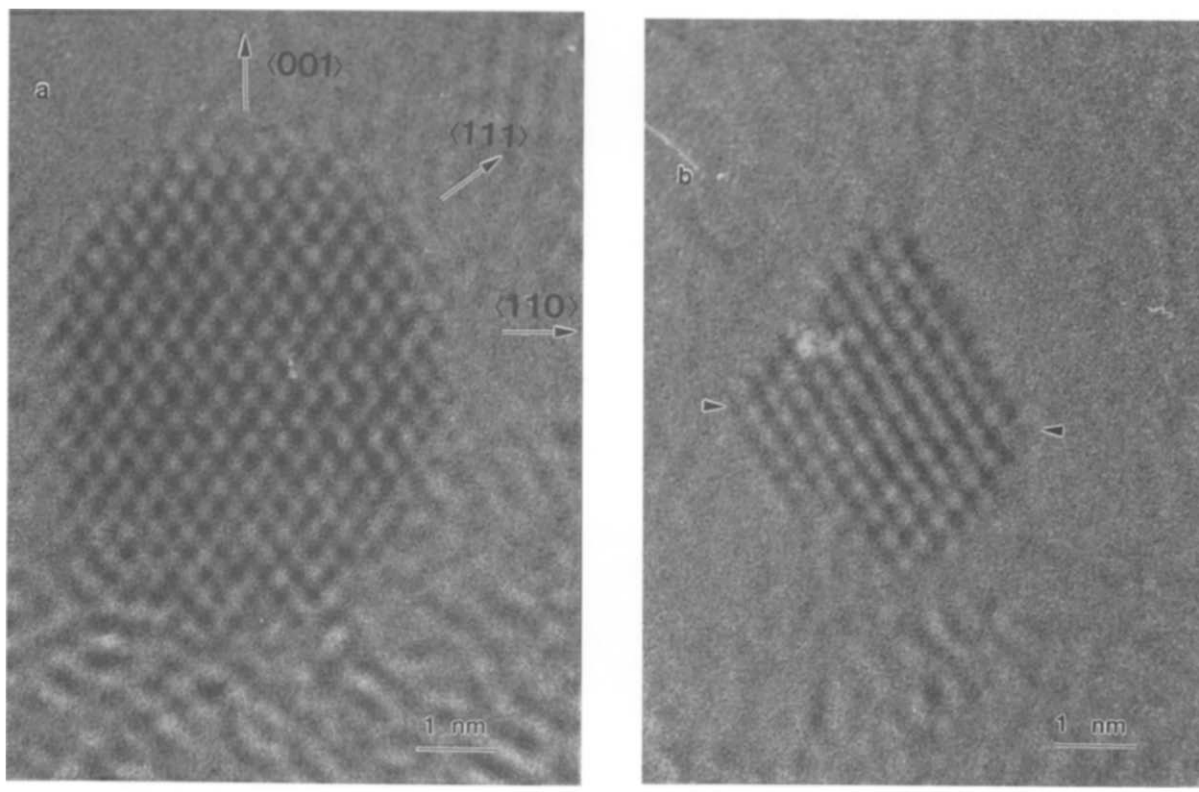

Fig. 2. (a) A perfect CeO_2 cuboctahedral particle oriented along ⟨110⟩ zone axis. The particle clearly shows the (111), (100) and (110) type-facets. (b) A quasi-perfect CeO_2 cuboctahedral particle oriented along the ⟨110⟩ zone axis showing a rounding off of (111) dihedra (arrows).

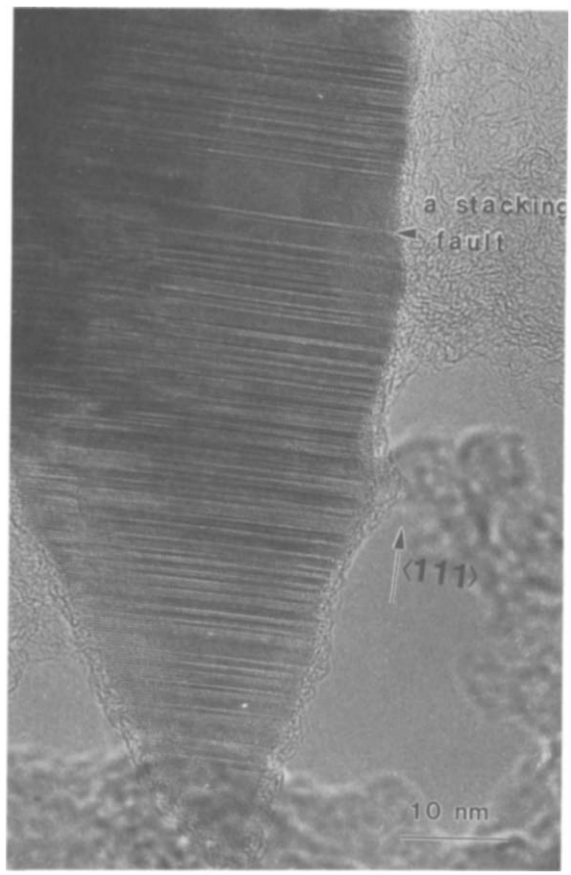

Fig. 3. A high-resolution electron micrograph showing a SiC crystallite oriented along the ⟨110⟩β-SiC zone axis. Note the abundance of stacking faults along the ⟨111⟩ direction.

off of (111) dihedra (Fig. 2b) can be explained by the fact that the (110) facets are the most orientationally unstable among the three mentioned type facets. Another fact that can be considered is the size of the cuboctahedral particle. For instance, it is well known that small gold particles (>1000 atoms) do not show any (110) faceting [16,17].

It can be concluded that the cerium doped active carbon precursor shows a good dispersion of CeO_2 particles over the active carbon. These CeO_2 particles were found to have an abundance of monoatomic (111) and (001) surfaces. On the other hand, the active carbon structure shows the formation of preferred orientation domains (white arrow in Fig. 1) arising from an ordering process due to the reorganisation of the active carbon's BSU (basic structural units). A detailed study concerning the growth of these domains as a function of heat treatment has already been reported in a previous publication [11].

3.2. Cerium doped silicon carbide

In a recent study [13], the characterisation of the Ce doped SiC catalyst support by means of X-ray diffraction (XRD) technique has shown the presence of the crystalline SiC as well as crystalline CeO_2 in small size, and in addition, the abundance of an amorphous phase. This amorphous phase was attributed to a Ce–SiC alloy in glassy structure form. In the present study, the use of the HRTEM technique can give a sense to the XRD interpretations by providing direct structural information and to then locate all of the above mentioned compounds.

As for the undoped support, the most striking feature of SiC crystallites is the abundance of stacking faults (Fig. 3). It is clear that the β-SiC polytype seems to be the one which grows most readily because of the multiplicity of the ⟨111⟩ rapid growth directions. Because of the low stacking fault energy (≈ 2 erg/cm^2 [18]) of (111) basal planes, the growth mechanism along the ⟨111⟩ direction will enhance the probability of occurrence of stacking faults. Consequently, any attempt to grow a β-SiC single crystal of large size usually results in mixtures of different polytypes or in what was already called either a heavily faulted β-SiC or a one-dimensionally disordered SiC polytype [12]. The lateral growth terminates with alternating {111} planes microfacets which represent at the thermodynamic equilibrium an energetically stable surface configuration because the surface energy of the close packed {111} planes is lower than that of the {112} planes. The SiC crystallites surface was often covered by an amorphous skin of vitreous silica due to an oxidation in air. In other regions, the crystalline SiC surface was also covered by a large amount of a new amorphous phase containing Ce, as shown in Fig. 4a. However, the presence of such a high amount of amorphous structure seems to indicate

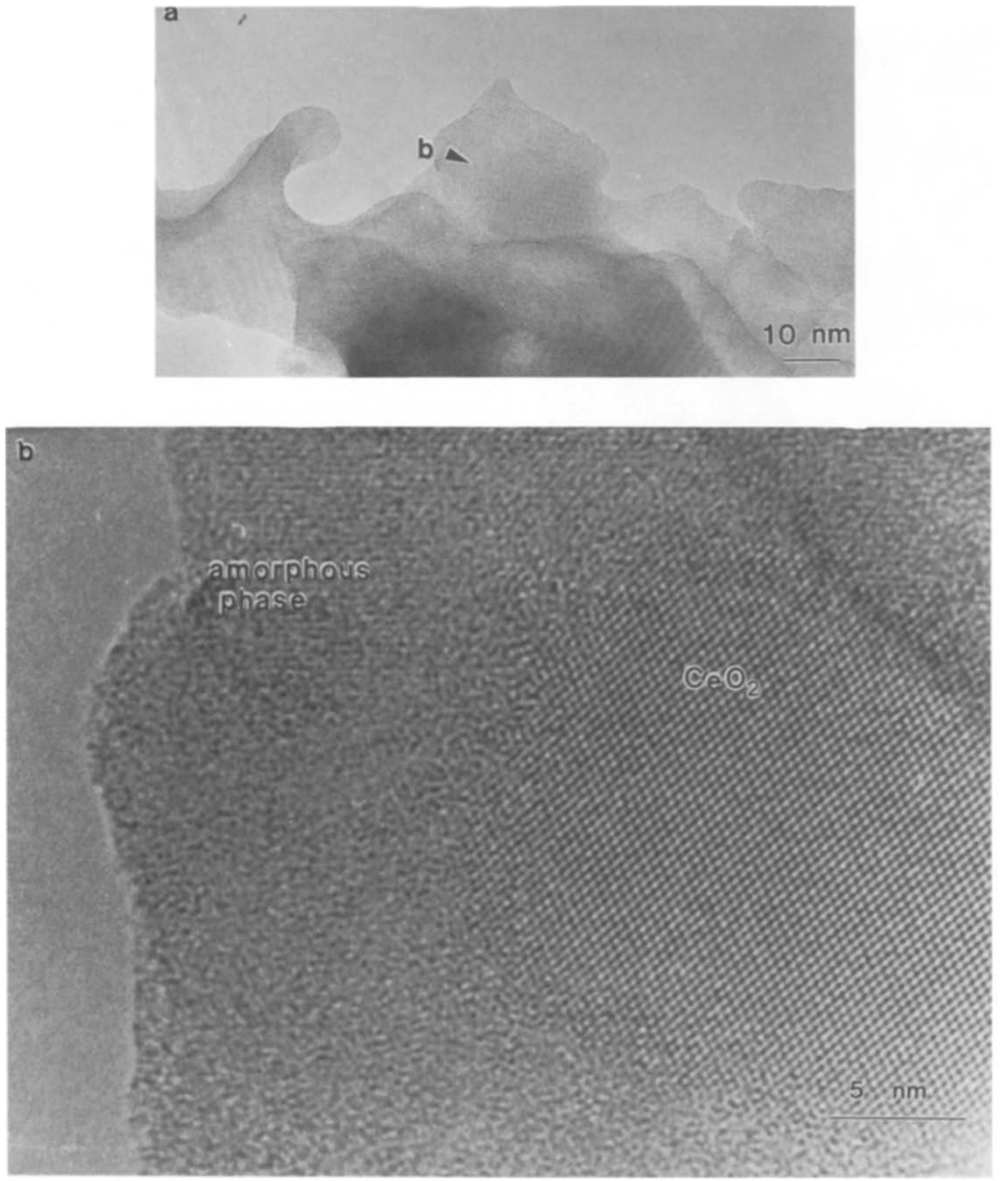

Fig. 4. (a) A low-magnification image showing a clear evidence of a large amorphous area. This amorphous phase is possibly a SiC–CeO_x complex alloy. (b) A high-magnification image showing the presence of a small area of crystalline CeO_2.

that its composition cannot contain Ce only since there is only 5 wt.-% of Ce. The hypothesis of an amorphous complex compound containing Ce and other elements such as Si and/or O can be put forward. Within these large amorphous areas, small crystalline CeO_2 domains were detected (Fig. 4b). The mean size of such particles is about 20 nm. It should be noted that, all this structural information agrees with the previous XRD data.

Very few rare earth silicate particles were also detected (see Fig. 5). Careful EDX quantitative measurements show that the compound is close to $CeSiO_5$. Extensive HRTEM simulations, using different rare earth silicate models, are on hand to

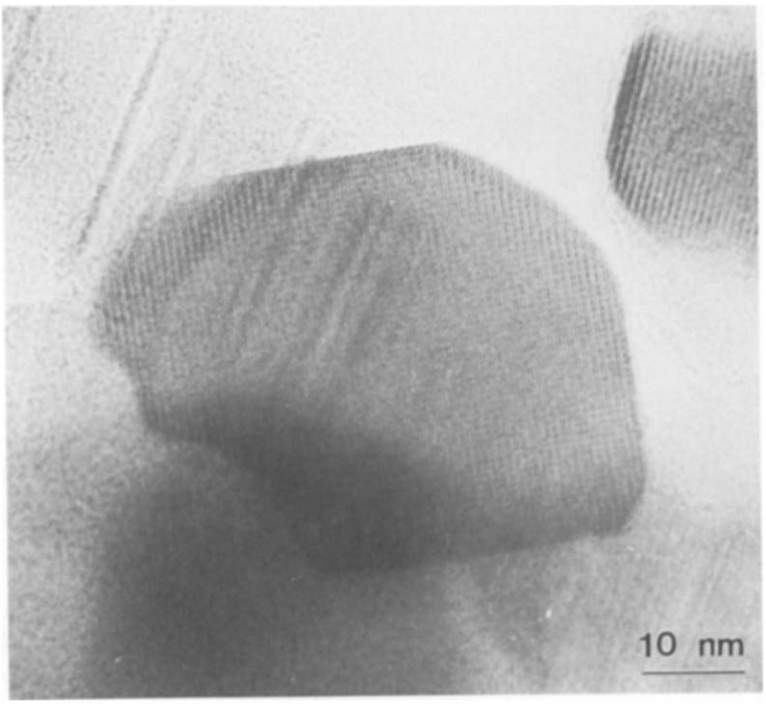

Fig. 5. A cerium silicate particle.

confirm the EDX measurements. Finally, during the growth of the cerium doped silicon carbide catalyst–support which has a granular form, another kind of SiC can be grown simultaneously in whisker form (Fig. 6). More details concerning the structure of these SiC whiskers are described in previous publications [19,20].

It was found that the Ce doped SiC catalyst–support contains a new compound which is a SiC–Ce amorphous phase. This result shows the interest of doping the active carbon before its use for the carbide synthesis.

3.3. Reduced Pt–Rh/SiC–Ce catalyst

After reduction under H_2 at 450°C for 2 h of the Pt–Rh/SiC–Ce catalyst, the cerium oxide is mainly present as CeO_2 in small particle form, with a mean size of about 30 nm (Fig. 7a). As for cerium oxide particles in cerium doped active carbon (above), it was generally possible to obtain high-resolution images of cerium dioxide in the ⟨110⟩ orientation taken at optimum Scherzer defocus, thus enhancing the 'dark atom' contrast. In this case (Fig. 7b), each dark contrast (or spot) represents three atomic columns: a cerium column with two oxygen columns on either side. Structurally speaking, the (001) type facet terminates either by Ce or O atom planes. The incomplete flatness of the (001) surface observed in Fig. 7b seems to indicate a pronounced structural change which can be attributed to the reductive treatment. This variation in the surface composition is consistent with previous results [4,21] indicating that under H_2 at 450°C, ceria is merely reduced at the surface and not in the bulk. The structure observed in Fig. 7b shows indeed that the bulk is unchanged.

Fig. 8a shows a micrograph of a Pt particle partially surrounded by a disordered discontinued surface film approximately 0.5 nm thick. No epitaxial relationship has been noted. Measurements of *d*-spacings from the optical diffractogram (Fig. 8b) show values equal to metallic Pt parameters, and EDX microanalyses performed on the surface film indicate the presence of cerium oxide.

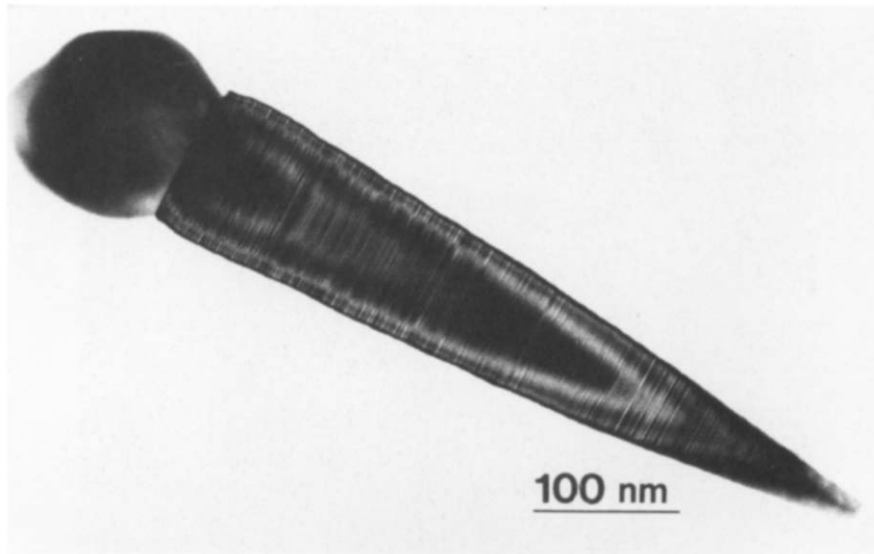

Fig. 6. A SiC whisker.

It is worth noting that the structure of the cerium oxide in interaction with Pt (Fig. 8a) is more disordered than that in interaction with Rh (Fig. 9a). This particular change in the structure results possibly from the interaction with Pt and so from a charge transfer from Pt to CeO_x. In the present study the origin of the disorder in the structure of the cerium oxide caused probably by the loss of oxygen from the parent fluorite CeO_2 is not further explored because of the complexity of the models which has to be considered. Oxygen vacancies must be taken into account to investigate the structures in the CeO_x system in order to improve the accuracy. On the other hand, the external shape of

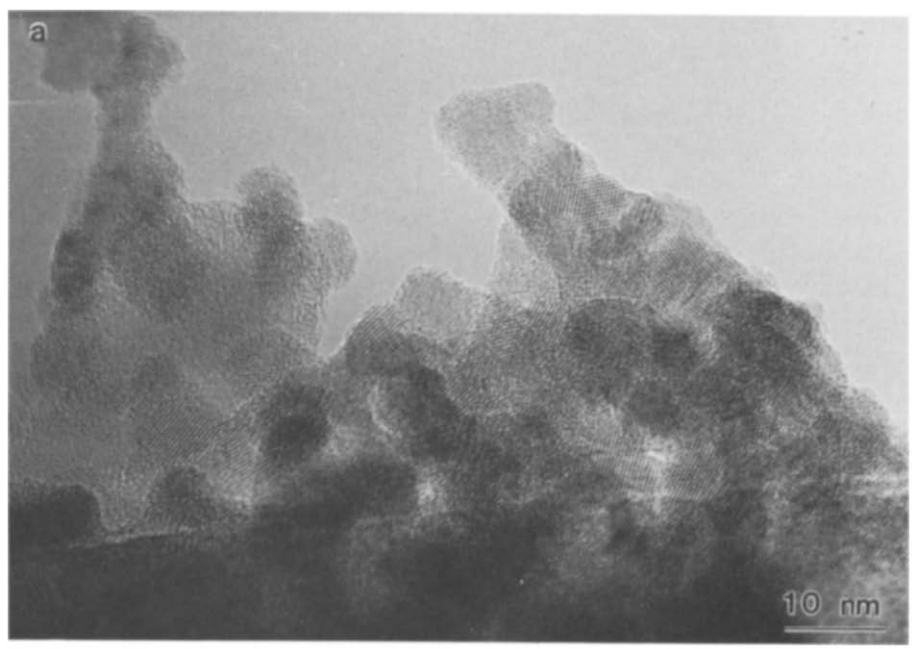

Fig. 7. (a) A high-resolution image of cerium oxide present in the reduced Pt–Rh/SiC–Ce catalyst. (b) A high magnification of a CeO_2 particle oriented along the ⟨110⟩ zone axis.

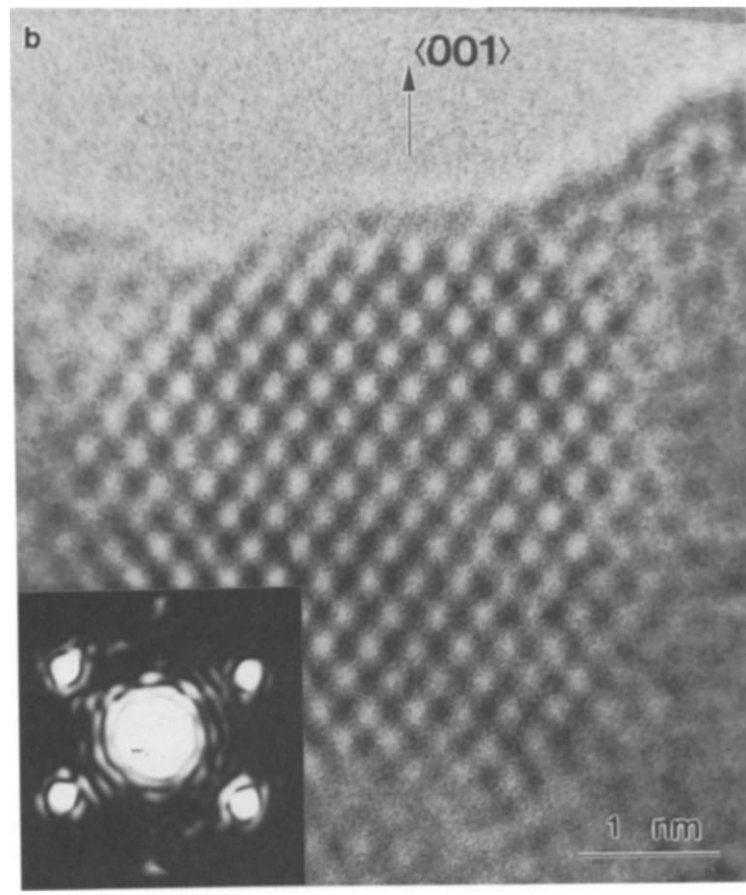

Fig. 7 (continued).

the Pt particle looks spherical and no faceting is observed. Taking into consideration the relatively large size of the particle (5 nm), the observed shape cannot be the result of a change in the bulk of the particle but probably due to the presence of cerium oxide, some rearrangement of atomic columns along the particle surface in contact with cerium oxide may occur, leading to changes in the external shape. Nevertheless, in the presence of a Pt/CeO_x interaction (Fig. 8a), the structural configuration is shown to be dependent on the nature of the noble metal [22]. Although the HRTEM images provide a realistic description of the actual configuration of the Pt/CeO_x interface, the physical and chemical natures of this interaction need further investigation in order to clarify and thus help understand the classical strong metal–support interaction (SMSI) reported in the literature dealing with Pt/CeO_2 [23,24].

Fig. 9a shows a micrograph of a Rh particle also partially surrounded by cerium dioxide (CeO_2) nanocrystals. These nanocrystals, as it can be noted from the optical diffractogram (Fig. 9b), are in epitaxial growth relationship with $Rh:(111)Rh//(111)CeO_2$.

In order to identify all the epitaxial relationships at these interfaces, high-magnification imaging was necessary. Two high-magnifications were done as shown in Fig. 10a and b. On the one hand, Fig. 10a (A) shows that the (111)Rh and $(111)CeO_2$ planes are parallel to the interface. In part B, no such a clear relationship can be observed. On the other hand, Fig. 10b (C) shows that Rh(111) and $(111)CeO_2$ planes are aligned.

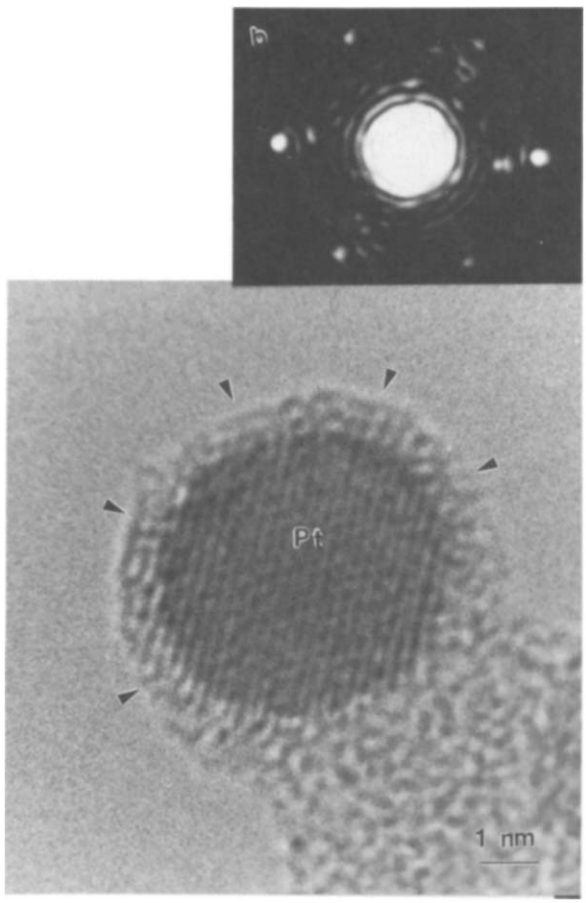

Fig. 8. A high-resolution image corresponding to a Pt particle partially surrounded by cerium oxide (arrows).

The misfit calculated from crystallographic consideration is about 34%, which implies that three (111)CeO_2 planes should grow parallel to four (111)Rh planes. On part D of Fig. 10b, the epitaxial relationship is similar to that deduced from the left side of Fig. 10a (part A). Following the intensities along the interfaces, the presence of an homogenous contrast can be observed, correlated to a very thin layer of about 0.2 nm thick. This very thin layer is actually an interface complex involving Rh–O–Ce [24]. This may be the result of the SMSI that many authors have reported in Rh supported ceria catalyst studies [25–27]. In fact, although much work has been done on the chemistry and structure of ceria used as a catalyst support, little attention has been paid to the same properties when cerium oxide is used as an additive. In terms of its activity, the addition of cerium oxide has shown similar improvements as in Rh/CeO_2 catalyst systems [13]. Basically, as for the SMSI configuration, the Rh/CeO_2 equilibrium configuration shown in Fig. 9a exhibits a preferred facets-type interaction rising from well defined growth sites. The CeO_2 nanocrystals in interaction with Rh does not show any drastic structural changes, at least in the bulk, after reduction under H_2 at 450°C. Probably the reduction slightly affects the surface of the nanocrystals as already mentioned above in the case of CeO_2 alone. While the interaction gives an active interface, or a buffer oxygen layer, formed at least by a single monoatomic layer, the chemistry of the interaction in presence of H_2 is still a matter of uncertainty. In recent investigations on Rh/CeO_2 catalyst [28,29], it has been reported that the adsorption/desorption rates of H_2 in presence of cerium oxide are sensitive to the dispersion of metals as well as to the pretreatment of the catalyst. Ceria has also a high ability to chemisorb large amounts of hydrogen. Besides, the chemisorptive properties of the Rh particles seems not to be inhibited at 500°C [27].

The low temperature oxidation/reduction feature demonstrated in the form of the light-off curves, and the improvement in the stabilisation of noble metals dispersion proved in a recent study [13], appear to be a synergistic oxidation/reduction of the (Pt+Rh)/CeO_x interfaces and some cerium oxide surfaces. However, the improvement in catalytic activity cannot be explained by oxygen storage only within the cerium oxide. The present HRTEM study on reduced Pt–Rh/SiC–Ce catalyst gives direct evidence of a selective association of Pt and Rh metals with the cerium oxide additive. The association, on the one hand, shows that cerium oxide is not inert towards noble metals, and on the other hand, it gives rise to a noble metal–cerium oxide composite of which the reduction is coupled. This particular interaction suggests that Pt and Rh selectively migrate to small cerium oxide particles during catalyst preparation. The formation of an active interface, or a buffer oxygen layer which can be defined as a

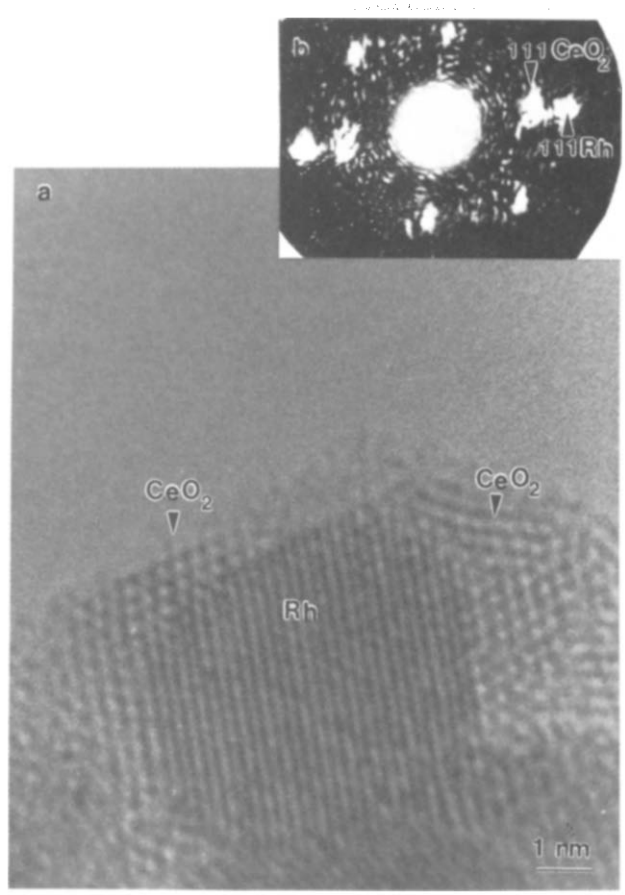

Fig. 9. A high-resolution image corresponding to a Rh particle supporting CeO_2 nanocrystals.

surface that serves as a common boundary between noble metals and cerium oxide, must be then considered to interpret the improvement in catalytic activities. In that case, one can propose that during reductive treatment, the ionised or re-oxidised vacancies, located at reduced cerium oxide surfaces in contact with reduced noble metals (NM) surfaces, can help the formation of such an interface complex involving NM–O–Ce.

3.4. Aged Pt–Rh/SiC–Ce catalyst

Fig. 11 shows a low-magnification electron micrograph illustrating the typical morphology of the Pt–Rh/SiC–Ce catalyst after it had been aged following the catalytic cycling processes b and c, described above. As one can observe, the SiC particle is partially covered by a number of cerium oxide particles (arrows). It is again observed, as for the reduced catalyst, that the cerium oxide is associated with the noble metals. This association is confirmed in high-magnification images, such as Fig. 12a which shows a Pt particle apparently supported on a cerium oxide layer of about 1 nm thick, which itself is supported on glassy silica covering SiC. Measurements from the optical diffractogram (Fig. 12b) performed on the Pt particle indicate that *d*-spacings correspond to Pt metallic state parameters. The formation of the platinum oxide at the Pt/CeO_x interface is rather difficult to predict from the electron micrograph. A part of the image (arrow) shows planes in the order of 0.35 nm, which can be attributed to the $(110)PtO_2$ structure. On the basis of previous work [6], the hypothesis putting forward the presence of surface PtO species does not agree with

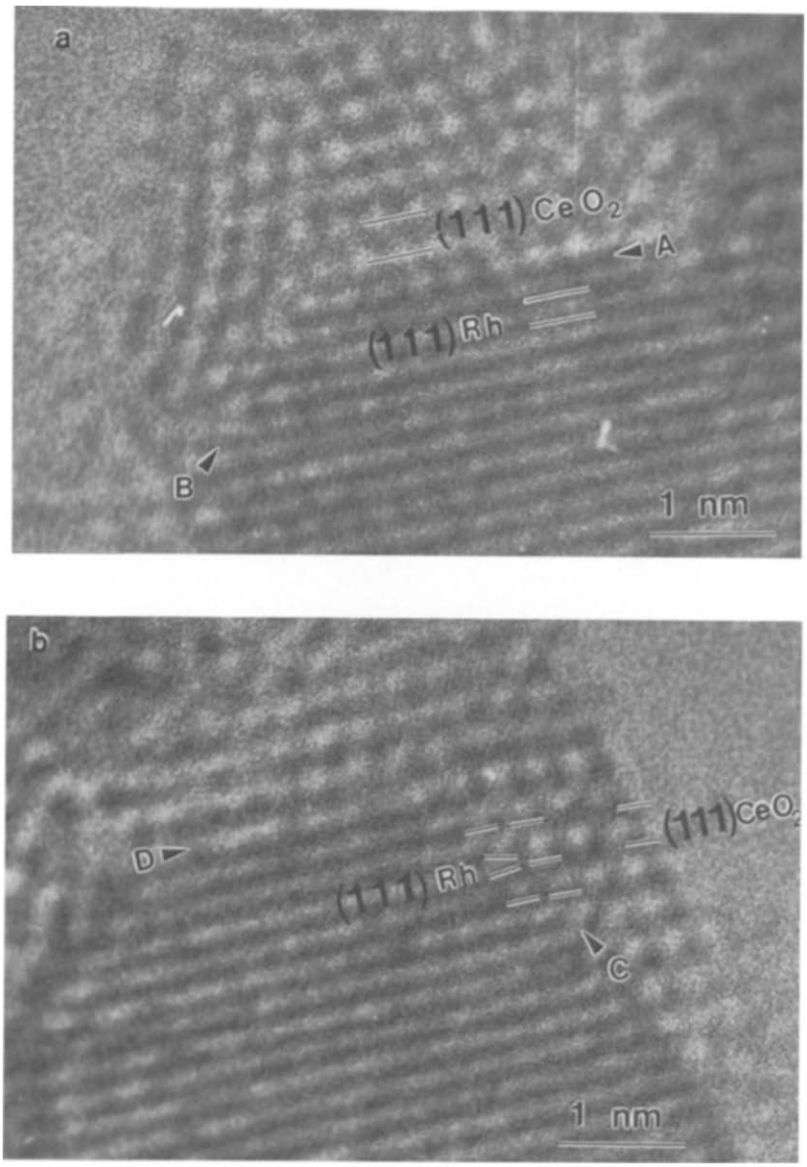

Fig. 10. High magnification images taking from Fig. 9 showing the growth epitaxial relationships between Rh and CeO_2.

the present HRTEM results. The surface of the Pt particle looks free from any oxide species. However, the existence of a platinum oxide layer at the interface was suggested by Serre et al. [30] to explain the destruction of a particular active interface between Pt and CeO_2 which results in the disappearance of the oxidation of CO directly by the oxygen of the cerium oxide situated at the proximity of the interface.

Another interesting example is shown in Fig. 13a. In this case, the cerium oxide is supporting a Rh particle. Aside from the intrinsic interest in the Rh–CeO_x interaction, there is an obvious structural change due to the catalytic cycling over the catalyst. A crystalline-to-amorphous transformation has occurred in a striking way within the cerium oxide structure at the Rh/CeO_x interface. This disorder in the CeO_x structure is a sufficient prove that CeO_x participates, co-operatively with Rh, in the gas conversion mechanisms. It also should be noted that, in contrast to the reduced catalyst, the Rh surface of the aged catalyst shows

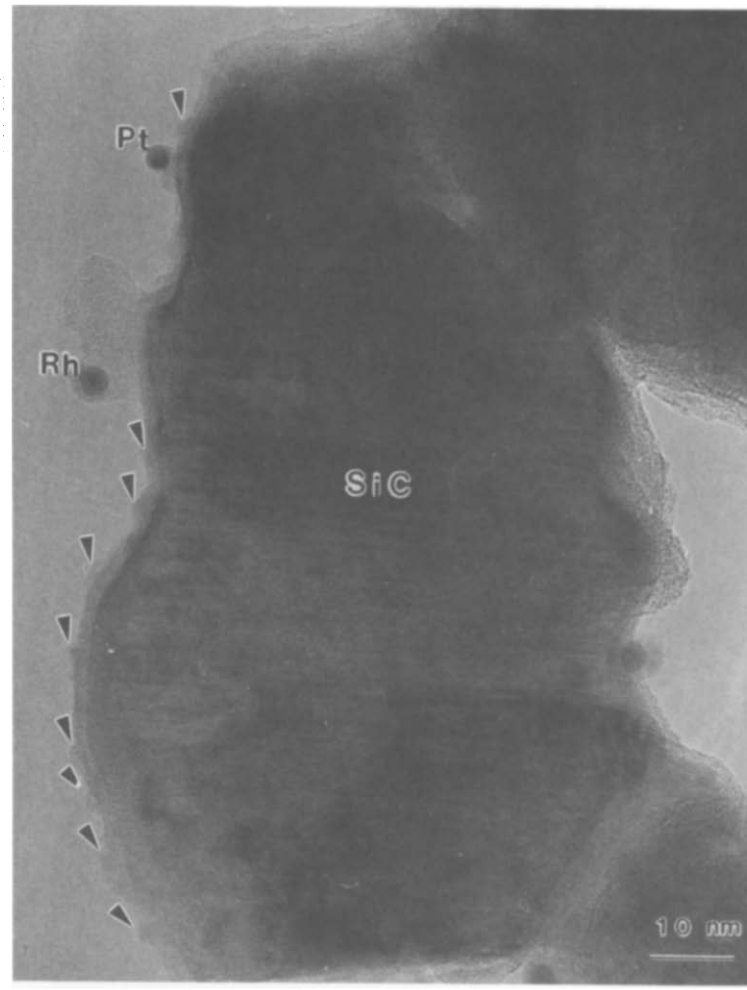

Fig. 11. A low-magnification image corresponding to the Pt–Rh/SiC–Ce aged catalyst The arrows indicate the presence of cerium oxide dispersed over the SiC particle.

the growth of a Rh sub-oxide phase formed by three to four monoatomic layers. The Rh sub-oxide phase grows parallel to the (111)Rh planes as shown in the optical diffractogram (Fig. 13b). Usually, the thermal decomposition of rhodium oxide gives rise to a mixtures of Rh_2O_3, Rh in its metallic state and a sub-oxide with RhO stoichiometry [31]. Following up a HRTEM study, Logan et al. [32] have reported the existence of a metastable rhodium oxide phase (RhO), with lattice spacing of about 0.29 nm, which grows on (111)Rh planes after oxidation at 500°C of the Rh/SiO_2 and Rh/TiO_2 catalysts. This suggestion was well-argued by an XPS result, previously obtained by Peuckert [33], who has shown the presence of a Rh oxidation state peak lower than Rh^{3+} (intermediate between Rh^{3+} and Rh^0). The proposed RhO phase consists of simple Rh and O plane alternation, which gives a fcc-like structure. The Rh surface oxidation is not surprising because it very well explains the decrease in NO conversion (see ref. [13]).

4. Concluding remarks

It must be emphasised that the SiC catalyst support represents a high chemical inertia since no

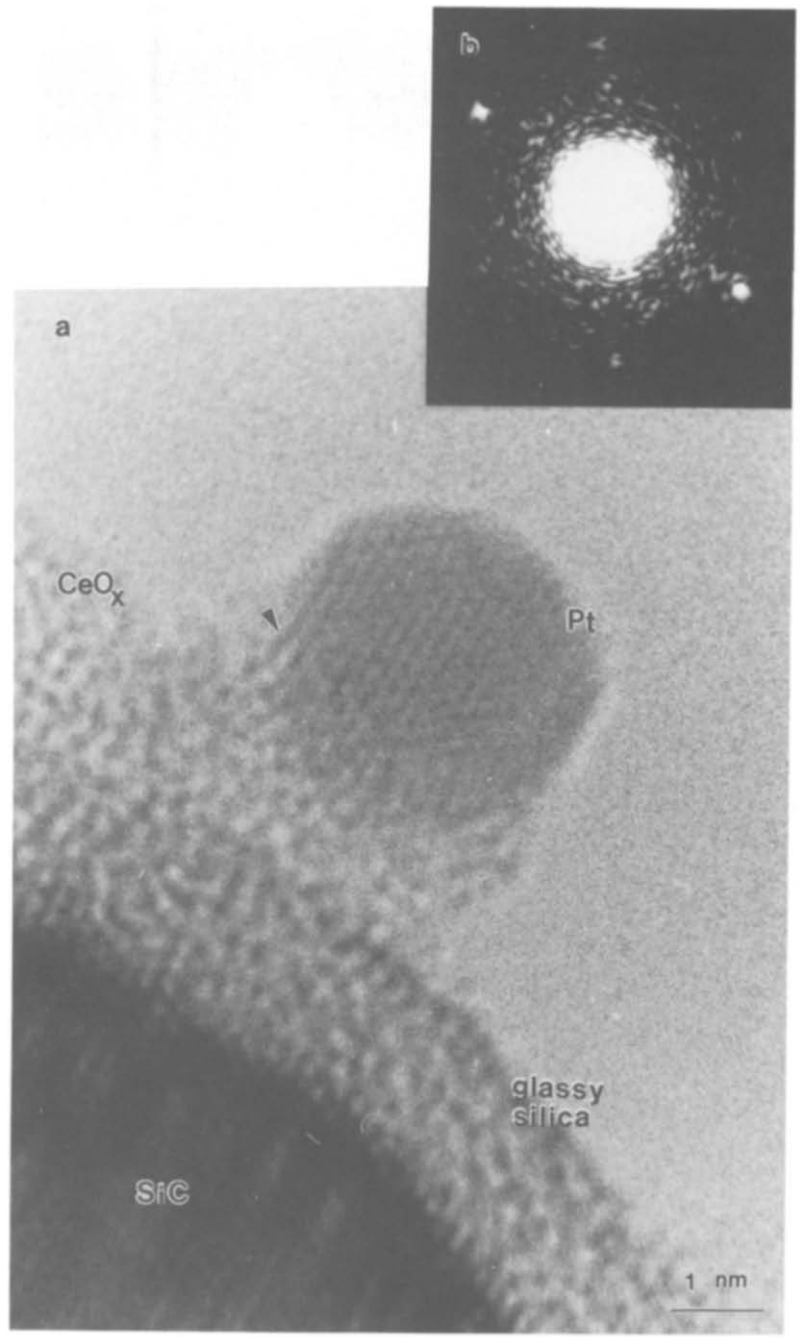

Fig. 12. A high-resolution image of a Pt particle after the ageing treatment of the catalyst.

structural modifications were observed on the noble metals caused by SiC. The recuperation of the active phase (Pt+Rh) is then possible by simple acid washing.

The previous laboratory reactor experiments with a Pt–Rh/SiC–Ce catalyst have shown that the addition of cerium oxide to the active carbon precursor before the synthesis of the SiC catalyst

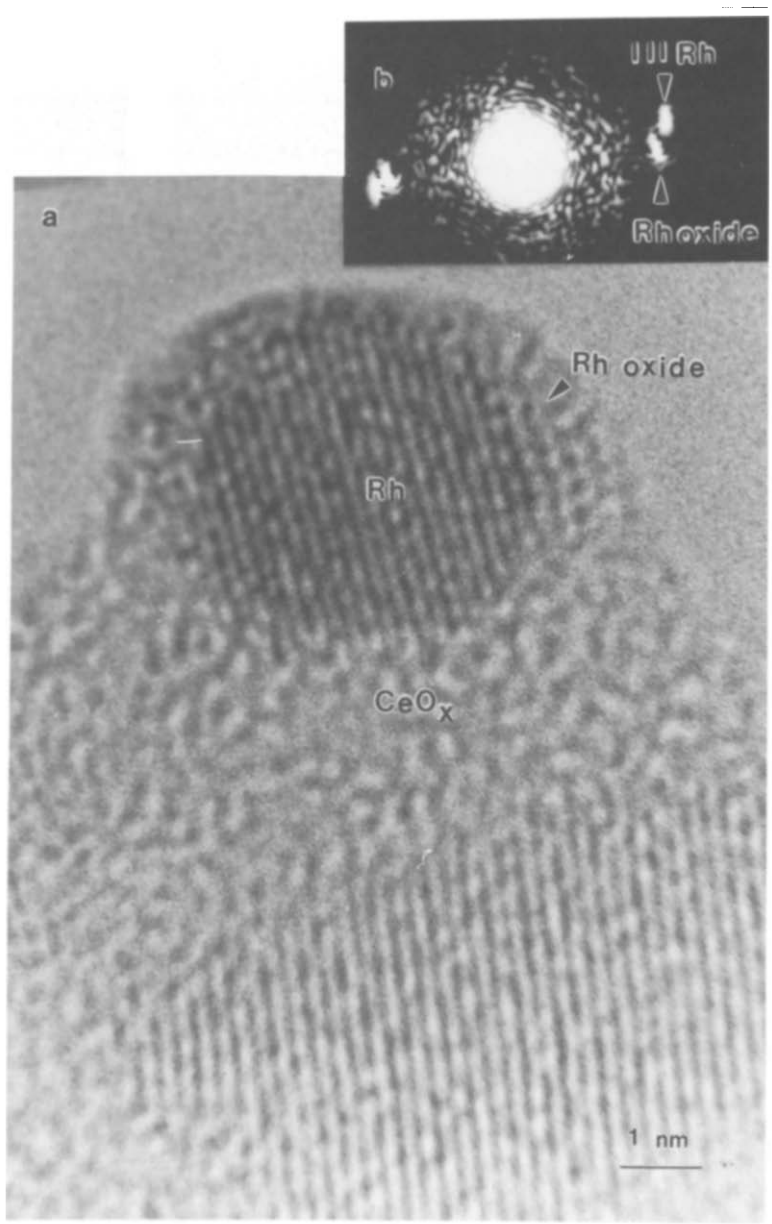

Fig. 13. A high-resolution image of a Rh particle after the ageing treatment of the catalyst. Note the formation of a Rh oxide over the Rh surface.

support results in an improvement in gas conversion and in a lower temperature activity. An overview of the HRTEM results gives clear evidence of the presence of an active interface resulting from a strong metal–additive interaction. This active interface plays a key role in the chemical reaction mechanisms. Cerium oxide can then catalyse a wide range of reactions (oxidation or reduction) on its own as a catalyst support and as an additive to enhance the activity of Pt and Rh catalyst systems, while the noble metals are electron donors or acceptors through the interface. Accordingly, the active phase is less affected by the catalytic cycling which extends the efficiency and life of the catalyst.

The present work reveals the power of ex situ HRTEM to characterise the sub-nm sized particles in the field of heterogeneous catalysis in order to

correlate the nanostructure of the catalyst with its catalytic performances. Unfortunately, one limitation not yet overcome, due to of the high vacuum required concerns *the dynamic study of heterogeneous chemical reactions within the electron microscope.* High-resolution in situ Controlled Atmosphere TEM (CATEM) of heterogeneous catalysts has been successfully performed in investigating the behaviour of ceria under flowing nitrogen gas at 20 Torr [34]. But no realistic experiments using exhaust gases were done. On the other hand, the level reached by in situ HRTEM, in a controlled manner such as by heating [35], is very promising for fundamental material reactions. Kinetic measurements can be made, as activation energies and kinetic laws, and the whole extent of a material transformation can be investigated in one sample; something that would take months of work if studied conventionally. The development of electron microscopes, and in particular combining direct in situ HRTEM observations of atomic behaviour with CATEM will lead to a greater understanding of gas/solid interactions at the atomic level in heterogeneous catalyst systems. Such improvements represent the major challenges for future work in TEM manufacturing.

Acknowledgements

This research was supported by the Péchiney Company. Gabrielle Ehret (IPCMS, Strasbourg) is gratefully acknowledged for her technical assistance.

References

[1] M.J. Ledoux, J. Guille, S. Hantzer and D. Dubots, European Patent No. 88420352.
[2] M.J. Ledoux, S. Hantzer, C. Pham-Huu, J. Guille and M.P. Desaneaux, J. Catal., 114 (1988) 176.
[3] H.C. Yao and Y.F. Yu Yao, J. Catal., 86 (1984) 254.
[4] Y.F. Yu Yao and J.T. Kummer, J. Catal., 106 (1987) 307.
[5] J.Z. Shyu, K. Otto, W.L.H. Watkins, G.W. Graham, R.K. Belitz and H.S. Gandhi, J. Catal., 114 (1988) 23.
[6] J.G. Nuan, H.J. Robota, M.J. Cohn and S.A. Bradley, in A. Crucq (Editor), Catalysis and Automotive Pollution Control II, Elsevier, Amsterdam, 1991, p. 221.
[7] A.F. Diwell, R.R. Rajaram, H.S. Shaw and T.J. Truex, in A. Crucq (Editor), Catalysis and Automotive Pollution Control II, Elsevier, Amsterdam, 1991, p. 139.
[8] J.C. Summers and S.A. Ausen, J. Catal., 58 (1979) 131.
[9] M.G. Sanchez and J.L. Gazguez, J. Catal., 104 (1987) 120.
[10] J.M. Hermann, E. Rameroson, J.F. Tempere and M.F. Guilleux, J. Catal., 53 (1989) 117.
[11] M. Benaissa, J. Werckmann, G. Ehret, E. Peschiera, J. Guille and M.J. Ledoux, J. Mater. Sci., 29 (1994) 4700.
[12] M. Benaissa, J. Werckmann, J.L. Hutchison, E. Peschiera, J. Guille and M.J. Ledoux, J. Crystal Growth, 131 (1993) 5.
[13] C. Pham-Huu, S. Marin, M.J. Ledoux, M. Weibel, G. Ehret, M. Benaissa, E. Peschiera and J. Guille, Appl. Catal. B: Environmental, 4 (1994) 45.
[14] H.D. Cochrane, J.L. Hutchison and D. White, Ultramicroscopy, 31 (1989) 138.
[15] R. Defay and A. Prigogine, in Surface Tension and Adsorption, Longman, New York, 1966, Ch. 17.
[16] S. Iijima and T. Ichihashi, Jpn. J. Appl. Phys., 24 (1985) L125
[17] S. Iijima, in S. Sugano, Y. Nishina and S. Ohnishi (Editors), Microclusters, Springer, New York, 1987, p. 186.
[18] R. Stevens, J. Mater. Sci., 7 (1972) 517.
[19] M. Benaissa, G. Ehret, J. Guille, J. Werckmann and E. Peschiera in Proceedings of Electron Microscopy, Vol. 2, 10th EUREM Granada, Spain, 1992, p. 381.
[20] M. Benaissa, J. Werckmann, G. Ehret, J. Guille and E. Peschiera, Interface Sci., 1 (1993) 91.
[21] M. Johnson and J. Mooi, J. Catal., 103 (1987) 502.
[22] M. Benaissa, C. Pham-Huu, M.J. Ledoux, J. Werckmann and J. Guille, in Proceedings of Electron Microscopy, Vol. 2B, 13th ICEM Paris France, 1994, p. 1073.
[23] P.J. Levy and M. Primet, Appl. Catal., 70 (1991) 263.
[24] R. Levy and M. Boudart, J. Catal., 32 (1974) 304.
[25] M. Pan, J.M. Cowley and R. Garcia, Micron Microscopica Acta, 18 (1987) 165.
[26] A. Trovarelli, G. Dolcetti, C. Leitenburg, J. Kaspar, P. Finetti and A. Santoni, J. Chem. Soc., Faraday Trans., 88 (1992) 1311.
[27] S. Bernal, J.J. Calvino, M.A. Cauqui, G.A. Cifredo, A. Jobacho and J.M. Rodriguez-Izquierdo, Appl. Catal. A: General, 99 (1993) 1.
[28] S. Bernal, J.J. Calvino, G.A. Cifredo, J.M. Rodriguez-Izquierdo, V. Perrichon and A. Laachir, J. Catal., 137 (1992) 1.
[29] S. Bernal, J.J. Calvino, G.A. Cifredo, J.M. Rodriguez-Izquierdo, V. Perrichon and A. Laachir, J. Chem. Soc., Chem. Commun., (1992) 460.
[30] Ch. Serre, G. Belot, F. Garin and G. Maire, J. Catal., 140 (1993) 1.
[31] L. Wohler and W. Müller, Z. Anorg. Chem., 149 (1925) 135.
[32] A.D. Logan, E.J. Braunschweig, A.K. Dayte and D.J. Smith, Ultramicroscopy, 31 (1989) 132.
[33] M. Peuckert, Surf. Sci., 141 (1984) 500.
[34] G.M. Parkinson, Catal. Lett., 2 (1989) 303.
[35] D.H. Ko and R. Sinclair, Ultramicroscopy, (1995), in press.